Nuclear Materials and Energy 20 (2019) 100689

Contents lists available at ScienceDirect

Nuclear Materials and Energy

journal homepage: www.elsevier.com/locate/nme

Retention properties in displacement damaged ultra-fine grain tungsten exposed to divertor plasma

J.L. Barton[a], D.A. Buchenauer[a], W.R. Wampler[b], D.L. Rudakov[c], Z.Z. Fang[d], C.J. Lasnier[e], J.A. Whaley[a], J.G. Watkins[a], E.A. Unterberg[f], R.D. Kolasinski[a,*], H.Y. Guo[g]

[a] Sandia National Laboratories, P.O. Box 969, Livermore, CA 94551, USA
[b] Sandia National Laboratories, P.O. Box 5800, Albuquerque, NM 87185, USA
[c] University of California San Diego, 9500 Gilman Drive, La Jolla, CA 92093, USA
[d] University of Utah, 201 President's Circle, Salt Lake City, UT 84112, USA
[e] Lawrence Livermore National Laboratory, 7000 East Avenue, Livermore, CA 94550, USA
[f] Oak Ridge National Laboratory, 1 Bethel Valley Rd, Oak Ridge, TN 37830, USA
[g] General Atomics, P.O. Box 85608, San Diego, CA 92186, USA

A B S T R A C T

One of the main advantages of using tungsten (W) as a plasma facing material (PFM) is its low uptake and retention of tritium. However, in high purity (ITER grade) W, hydrogenic retention increases significantly with neutron-induced displacement damage in the W lattice. This experiment examines an alternative W grade PFM, ultra-fine grain (UFG) W, to compare its retention properties with ITER grade W after 12 MeV Si ion displacement damage up to 0.6 dpa (displacements per atom.) Following exposure to plasma in the DIII-D divertor, D retention was then assessed with Nuclear Reaction Analysis (NRA) depth profiling up to 3.5 μm and thermal desorption spectrometry (TDS). Undamaged specimens were also included in our test matrix for comparison. For all samples, D release peaks were observed during TDS at approximately 200 °C and 750 °C. For the ITER-grade W specimens, the intensity of the 750 °C release peak was more pronounced for specimens that had been pre-damaged. Conversely, UFG samples that had been damaged by 12 MeV Si showed enhancement of the lower temperature release peak (200 °C). NRA profiles also reveal a higher D concentration for UFG W samples up to the peak in the damage profile at a depth of 2 μm. Overall, we observed that the total trapped inventory in UFG W was 20% higher than ITER grade W in the undamaged case and 10% higher in the damaged case. A comparison of NRA and TDS data indicates that a larger fraction of the total retained D is trapped near the surface (86–100%) in UFG W pre-damaged to 0.6 dpa compared with ITER grade W (39–61%). Further examination of the UFG material with microscopy is recommended for a definitive determination of the types of defects responsible for D trapping. Our results highlight some potential trade-offs associated UFG W regarding its performance from a tritium retention standpoint. That said, our TDS results indicate that this enhanced inventory can be released by baking at relatively low temperatures (< 500 °C), providing an avenue for minimizing tritium retention in this material that would be practical for implementation in a tokamak.

1. Introduction

Lattice defects in plasma facing materials (PFMs) can trap hydrogen isotopes, removing tritium from the fuel cycle and eventually causing radiation safety concerns [1]. Understanding how trapping at displacement damage created by 14 MeV fusion neutrons affects tritium retention is an important consideration for plasma-facing materials and has been a topic of considerable recent study [2]. Much of this work has focused on tungsten (W), in part because it has been selected as the divertor material for the ITER tokamak. Furthermore, it is considered a leading material for future fusion devices because of its high melting point, low coefficient of thermal expansion, low sputtering yield, and its low hydrogen solubility [3]. Depending on the irradiation and plasma-exposure conditions, damage caused by neutrons can significantly increase retention in high energy traps, which requires W to be heated to high temperatures (> 500 °C) to remove trapped hydrogen [4–6]. It is important to note that much of this prior work has been conducted on single crystals, recrystallized W, and warm-rolled ITER-grade W specimens [7]. Given the recent efforts focusing on development of tungsten alloys and composites [8–10], understanding tritium trapping at displacement damage in these new materials is an important consideration that has not been adequately explored.

The development of ultra-fine grained (UFG) W has received considerable recent interest, with several research groups producing and testing new materials [11–14]. This class of W materials has a microstructure characterized by small (< 1 μm) grains with transition metals or carbides as dispersoid particles at the grain boundaries. The dispersoids are intended to inhibit the grain growth and recrystallization embrittlement in W. Thermal fatigue loading [15] and thermal shock tests [16] with high heat fluxes from electron beams have demonstrated

* Corresponding author.
E-mail address: rkolasi@sandia.gov (R.D. Kolasinski).

https://doi.org/10.1016/j.nme.2019.100689
Received 30 July 2018; Received in revised form 3 May 2019; Accepted 15 May 2019
Available online 10 July 2019

that UFG W has improved resistance to thermal damage compared to ITER grade W, showing no significant cracking or roughening. UFG W has also been found to better handle thermal shocks under certain orientations [17]. Plasma gun deuterium loading experiments suggest the large density of grain boundaries may provide sinks for displacement damage caused by high energy Cu ions [11]. However, the conclusions from this work were not considered definitive because the authors could not eliminate the possibility that the high concentration of implanted Cu also affected the retention. In prior work by our research group, high plasma flux/fluence experiments in the PISCES linear device reveal that although deuterium retention is higher in UFG W, the surface morphology of UFG W is unchanged compared to the blisters and bubbles on the ITER grade W [18]. In addition, our previous gas-driven permeation measurements revealed elevated permeability for UFG W compared with conventional polycrystalline material [19]. Thus, we are motivated to study these effects combined, where heat flux, plasma flux, and displacement damage may have synergistic effects in a tokamak divertor.

This study focuses on an analysis of the hydrogen isotope retention in ion-damaged UFG W, including comparisons with more conventional ITER-grade W material. The samples were exposed to high-flux D plasmas in the DIII-D divertor using the Divertor Materials Evaluation System (DiMES) platform. To our knowledge, this represents the first such exposure of damaged UFG material in a relevant divertor environment. Our paper begins with a discussion of the microstructural characteristics of the UFG material along with a summary of sample preparation. This includes the experimental parameters used to pre-damage the specimens with 12 MeV Si ions as a surrogate for fusion neutrons. The sample exposure conditions in the DIII-D divertor are then discussed. A summary of retention results from nuclear reaction analysis (NRA) and thermal desorption spectroscopy concludes the paper.

2. Experimental

2.1. Sample preparation

The samples used in this experiment were bulk ITER grade tungsten [20] from Sumitomo Electric USA and bulk UFG tungsten manufactured at the University of Utah. The UFG W was created by a unique powder metallurgy process with W and titanium (Ti) powders, further details of which can be found in Ref. [12]. Small quantities of Ti particles (dispersoids) (1% wt.) were introduced as a means of inhibiting grain growth. In our prior work, we performed X-ray photoelectron and Auger spectroscopies to analyze the surface composition of the UFG W and electron microscopy to examine its microstructure [18]. Focused ion beam profiling and scanning electron microscope imaging revealed Ti dispersoids of approximately 100 nm in diameter that were present at W grain boundaries. Using electron backscatter diffraction mapping, we were able to determine the median grain size by reconstructing the grain boundaries using a 10° misalignment threshold. The areas of the individual grains were calculated and related to an equivalent diameter (e.g. the diameter of a circle with the same area.) Using the methods outlined by Minghard et al. [21], we histogrammed the grains according to their equivalent diameter, yielding a median grain size of 960 nm. No obvious orientation preference was noted from the EBSD orientation data. Auger and x-ray photoelectron spectroscopies shoed that these Ti dispersoids were in the form of TiO_2 [18]. These bulk samples were machined to have a 6 mm diameter exposure surface and 2 mm thickness. Samples were then polished mechanically to a 10 nm rms roughness, as measured by atomic force microscopy. Finally, all specimens were cleaned in acetone, followed by an ethanol ultrasonic bath, and then baked in 10^{-4} Pa vacuum to 1000 °C for one hour to stress relieve damage introduced by the mechanical polishing.

Displacement damage was done at Sandia National Laboratories using a silicon (Si) ion beam. The procedure is similar to a previous displacement damage experiment [22], where a 12 MeV Si^{++} beam is rastered across one sample in order to induce damage uniformly. We pre-damaged two ITER grade and two UFG W samples to 0.6 dpa (displacements per atom) using 90 nA of current up to a total fluence of 5×10^{18} Si/m^2. The damage profile vs depth is predicted using SRIM software [23] with a displacement damage threshold set to 40 eV and is shown in Fig. 5 as a dashed line. One of the UFG W samples received a larger, unknown fluence when the charge counter was started a short time after beam exposure began. With a reduced current of 30 nA, we damaged one UFG W sample with 0.06 dpa with a fluence of 5×10^{17} Si/m^2. The amount of implanted Si in these cases are small compared to the residual impurities already present in the samples and should not affect D retention results. All samples were mounted on the same stage during irradiation and were approximately room temperature. A complete listing of the different samples included in this study, along with the level of damage in each, is included in Table 1.

Table 1
Retention summary of all samples, where the samples with the closest temperature histories are highlighted in bold. The total retention is calculated from TDS data. We calculate the percent within 3 μm by taking the ratio of the integrated NRA retention data and the total retention. (*This sample's total retention is calculated from the NRA data. For clarity, the TDS data for this sample is left off, since it was measured with the electron multiplier off and cannot easily be compared to the other samples.).

Material type	Location	dpa	Total retention [$\times 10^{20}$ D/m^2]	% within 3 μm	Retained after heating to 500 °C [$\times 10^{20}$ D/m^2]
ITER	outer	0	2.04	25	1.59
ITER	middle	0.6	1.96	61	1.41
ITER	inner	0.6	3.63	39	2.89
UFG	middle	0	2.44	40	1.74
UFG	middle	0.06	1.89*	–	–
UFG	inner	0.6	3.98	100	0.92
UFG	outer	>0.6	3.75	86	1.87

2.2. Exposure in the DIII-D divertor

The DiMES platform is used to simultaneously expose damaged and undamaged samples to DIII-D plasma in the lower divertor. The DiMES stage has a graphite cap that clamps the samples down to a spring loaded base to help maintain thermal contact. Samples are oriented as in Fig. 1 spaced evenly on the 5 cm diameter cap with 6.5 mm between each sample. Plasma flow is in the direction indicated by the red arrow, showing the direction of the toroidal magnetic field (B_T), and the outward radial direction (R) is also indicated. Since some samples have redundant properties, we will use their radial locations on the DiMES stage for unique identification. The two samples closest to the strike point (i.e. at a more inner radius) are referred to as “inner”, the next column of three samples are referred to as “middle”, and the two outermost samples are referred to as “outer”.

There are several diagnostics near DiMES used to measure plasma and material properties. Langmuir probes located about 50 cm toroidally downstream from the DiMES location measure plasma densities, temperatures, and particle fluxes. Since we repeat the same discharge settings for every plasma shot, we initially sweep the outer strike point (OSP) radially outward over several probes to get radial profiles of plasma parameters and assume the profile is unchanged for the subsequent discharges using a steady OSP. There is a spring loaded type E thermocouple pressed against the back side of the middle sample to verify the temperatures measured by the infrared camera between discharges. The infrared camera (IRTV) views DiMES from the top of the machine sampling at 126.33 frames per second with a 0.2 ms integration time before, during, and after each discharge. Each pixel views approximately 0.05 mm^2 of the divertor, and the average intensity from a 5 × 5 grid of pixels (1.25 mm^2) is used to measure the

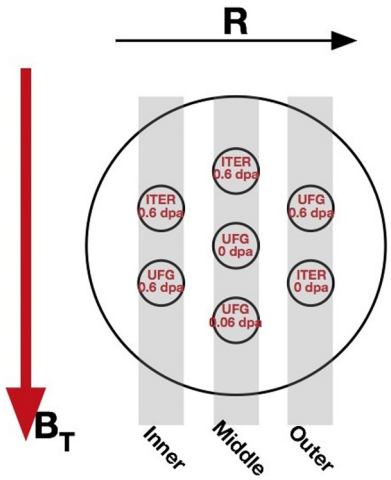

Fig. 1. Illustration of DiMES viewed from the top showing the ITER grade and UFG W sample locations. Arrows indicate the radially outward direction (R) and the plasma flow/toroidal magnetic field direction (B_T). The outer strike point of the plasma is approximately at the location of the B_T arrow, so we label three radial regions on the DiMES probe as "inner", "middle", and "outer".

surface temperatures of the samples. Before plasma exposure, the IRTV is calibrated between 86 and 335 °C using a heated DiMES stage with an ITER grade W sample.

We exposed the samples to ten similar L-mode deuterium (D) plasma discharges in the DIII-D tokamak. A sweeping OSP is used to get the flux profiles shown in Fig. 2 measured by the Langmuir probes while the DiMES stage is recessed from the divertor surface. The green fitted line is as a result of an asymmetric Gaussian, typically used for divertor profiles. We then raised the DiMES stage to the surface and exposed the samples to ten steady OSP discharges. The vertical line in Fig. 2 indicates the OSP location. During shots with a steady OSP, the shaded columns in the figure show the inner, middle, and outer locations of the samples relative to the OSP location. The particle flux radial profile is essentially uniform across the inner and middle columns of samples, and the outer column has approximately less than 6% lower flux compared to the peak value. The peak particle flux is 1.75×10^{22} D^+/m^2s, assuming only singly charged deuterium ions. Using the same flux value for each discharge, ten four-second discharges then will give a total D fluence of 7×10^{23} $/m^2$. Heat flux is calculated using the electron temperature and ion saturation current with a sheath heat transmission coefficient equal to 7 as in [24]. The heat flux profile peaks at 0.57 MW/m^2 near the middle region of

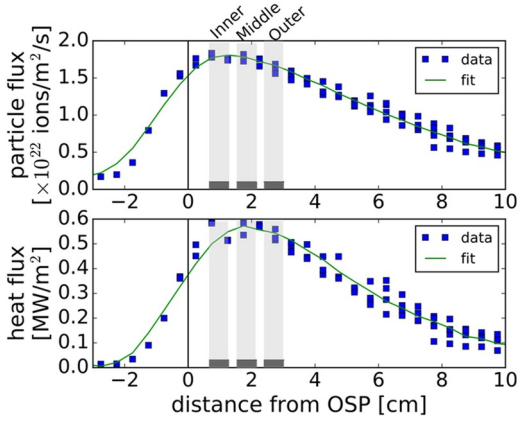

Fig. 2. Particle flux (top) and heat flux (bottom) radial profiles measured by Langmuir probes. The shaded regions indicate the inner, middle, and outer radial locations of our samples relative to a steady OSP. All samples receive particle and heat fluxes within 10% of the peak flux values.

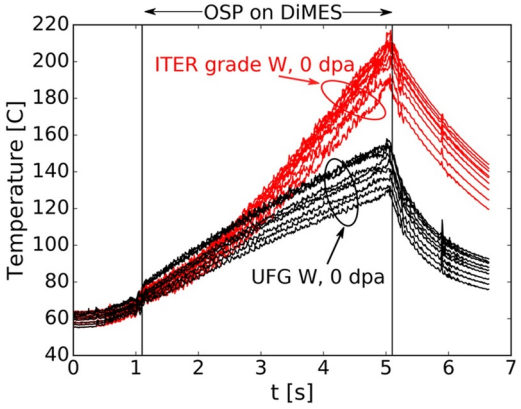

Fig. 3. IRTV temperature measurements during all plasma discharges on the ITER grade, 0 dpa, outer sample and the UFG W, 0 dpa, middle sample. Both samples are initially in thermal equilibrium, but the ITER grade sample seems to have decreased thermal contact with the DiMES cap and begins to heat more rapidly during the discharge.

buttons and is within 10% of this value across all samples. Using 1-D collisionless sheath theory, we calculate the D ion energy to be ~ 100 eV.

Although the heat fluxes were approximately uniform across all of the samples, the surface temperatures of the samples varied significantly. The DiMES stage is designed to spring load the samples against the graphite cap/heat sink; however, the IRTV indicate that some samples may have reduced thermal contact with the cap during the discharge. Fig. 3 shows an example comparing the two undamaged samples' temperature histories over all discharges. The temperatures of the two samples at the beginning of the discharge ramp up in a similar way until one of the samples begins to heat more rapidly. Since the two samples received about the same heat flux, it is likely that the rapid heating is due to reduced contact with the cap. To illustrate the differences in temperatures among all the samples, Fig. 4 shows the samples' surface temperature at the end of each discharge throughout the experiment. There is one UFG W sample (0.06 dpa, middle) and two ITER grade samples (0.6 dpa, inner and 0 dpa, outer) that have markedly higher temperatures than the other samples. Since all three of

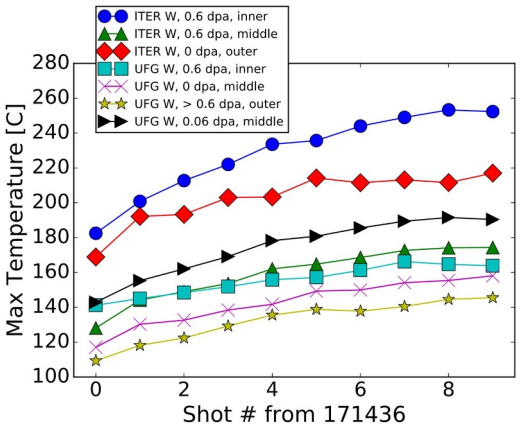

Fig. 4. Peak temperature of each sample at the end of every discharge. Samples having peak temperatures within 120–160 °C range have fairly good thermal contact with the DiMES cap; however, the 0.06 dpa UFG W sample (black side-triangles) and two ITER grade W samples (circles and diamonds) are heated significantly more throughout the plasma exposure. The two samples with the closest temperature histories are the ITER grade W, 0.6 dpa, middle sample (green triangles) and the UFG W, 0.6 dpa, inner sample (cyan squares). (For interpretation of the references to color in this figure legend, the reader is referred to the web version of this article.)

those samples are at different radial locations, we conclude that loss of thermal contact with the heat sink caused the rapid heating. The other samples' temperatures only have a 30 °C spread at the end of the discharge, likely due to differing thermal contact with the DiMES cap among the samples. Two samples have nearly the same temperature history, the 0.6 dpa ITER grade sample in the middle location and the 0.6 dpa UFG W sample at the inner radius location. Thus, we emphasize the comparison of these two samples. We also note that Fig. 4 shows a monotonic increase in temperature of each sample after subsequent discharges. There is only about 15 min between plasma shots, which is not long enough for DiMES to cool down to its initial temperature. However, we observe that the temperature of the DiMES cap and samples at the beginning of the discharges are in equilibrium and increased less than 10 °C from the first to last discharge (see Fig. 3 data near $t = 0$).

2.3. Quantification of D retention

After plasma exposure, the samples' deuterium retention is measured with nuclear reaction analysis (NRA) for concentration depth profiles up to 3.5 μm from the surface. A 2.5 MeV beam of ^{3}He ions is used to produce the D(^{3}He,p)α nuclear reaction in our samples. We measure the energy spectra (yield versus energy) of the protons with a 300 mm^2 silicon surface barrier detector close to the sample with an annular geometry to minimize kinematic broadening of the energy resolution. To stop elastically scattered ^{3}He from reaching the detector, the detector surface is covered with a 12 μm thick mylar foil. The incident ^{3}He ions lose energy as they scatter within the sample, so by energy and momentum conservation, the energy of the proton created deeper within the sample has a higher energy than the proton produced nearer to the surface. Thus, we convert the measured proton energy to a depth scale. This conversion is done with the SIMNRA program [25]. Yield counts are converted to D concentration using a SIMNRA simulated spectrum of uniform concentration D/W = 0.001, which is small enough to not significantly impact the stopping power. The ratio of measured to simulated counts times the D concentration used in the simulation gives the measured concentration. We also calibrated our sensor with a ErD standard sample with a known uniform D concentration.

The samples are then analyzed with thermal desorption spectroscopy (TDS) to understand trapping energetics and to measure total retention. Samples are heated at a constant rate of 0.5 °C per second in vacuum with a base pressure of 10^{-4} Pa, and a residual gas analyzer measures the partial pressures of H_2, HD, and D_2 molecules. A temperature ramp with an empty vacuum chamber is used to get background pressures, and a 2.4×10^{-11} D_2 mol/s leak standard is used to calibrate the pressure signals. With the exception of the 0.06 dpa UFG W sample, all measurements including the background measurement and the calibration had the electron multiplier turned on to amplify the measured signal and reduce noise. The HD flux and the D_2 flux are used together to give the total atomic D flux from each sample. We integrate the flux signal from the time the sample is 50 °C to the time the sample reaches 1000 °C to give the total D retention.

3. Results and discussion

The depth profiles measured by the NRA technique are shown in Fig. 5 along with the predicted displacement damage profile (calculated by SRIM) indicated by the dashed line. Damaged ITER grade W has an increased amount of D trapping up to 1 μm from the surface compared to the undamaged case and shows a 66% increase trapped D concentration over this depth. However, the damaged ITER grade samples do not have a significant increase in inventory near the peak in the damage distribution at 2 μm. This result is consistent with a previous displacement damage study that had W samples at low temperature (≈ 200 °C) during plasma exposure [4,26].

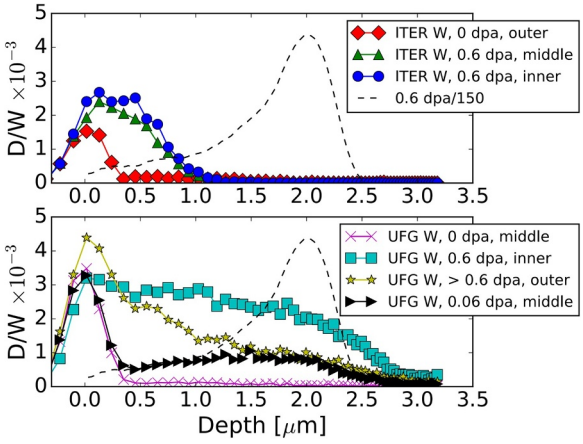

Fig. 5. Atomic fraction of D vs depth of the ITER grade W samples (top) and the UFG W samples (bottom). The 0.6 dpa damage profile predicted by the SRIM simulation is overlaid on both plots. All damaged samples have an increased D fraction, but UFG W samples have a higher D inventory throughout the damage region.

The lower panel of Fig. 5 shows the D concentration profiles in the UFG W samples. We first consider the "near surface" D concentration, defined here as the peak in the NRA depth profiles centered at 0 μm. For both the damaged and undamaged samples, the concentration at this point is comparable, reaching a maximum of 3×10^{-3} D/W. The outlier in our data set is the sample with >0.6 dpa, where the trapped concentration is about 30% higher. The differences in retention between the samples become more obvious at greater depths. For example, the damaged UFG W samples are populated with significantly more D extending beyond the peak in the damage distribution at a 2 μm depth. The 0.06 dpa UFG W specimen, corresponding to the lowest damage level, trapped 2.5 times less D than the 0.6 dpa UFG W at the depth where the damage distribution reaches a maximum. On the other hand, the sample with a slightly higher damage level (>0.6 dpa) retains approximately the same inventory as the 0.06 dpa sample at the same depth. One possible explanation for this difference is the different location (and therefore different temperatures) of each sample. The >0.6 dpa UFG W sample was in the "outer" position, and as a result was 30 °C cooler than the 0.6 dpa sample. This would have the effect of modestly reducing the diffusivity during plasma exposure. The differences we observe in the depth distribution of D in the >0.6 dpa sample could also be due to the larger level of displacement damage.

Comparing the NRA data of the UFG W to ITER grade W samples, we see a larger near-surface D inventory in undamaged UFG W and increased D trapping at greater depths in damaged UFG W. The near-surface trapped D concentration is 2.3 times higher in the undamaged UFG W compared with the ITER grade material. Both undamaged samples exhibit a sharp decline in retention around 400 nm, but this profile changes markedly after undergoing displacement damage. The 0.6 dpa UFG W sample (located at the "inner" position) had approximately the same temperature history as the 0.6 dpa ITER grade specimen located at the "middle" position. We see that 3.3 times more D is trapped in the damaged UFG W sample by populating the damaged created defects beyond the first 1 μm. This difference raises some questions about the nature of diffusion and trapping in the two materials following ion damage. The 12 MeV Si ions create Frenkel pairs within the lattice, leaving a vacancy and a W interstitial. Vacancies in W are known to have large trapping energies around 1 eV [27,28]. Such traps will not reach chemical equilibrium with D in solution until temperatures >500 °C are reached [29]. This means that D trapping is strong relative to solution sites during low temperature exposure, and the filling of traps can be calculated analytically using models described in Ref. [29]. Whereas the NRA technique shows the concentration

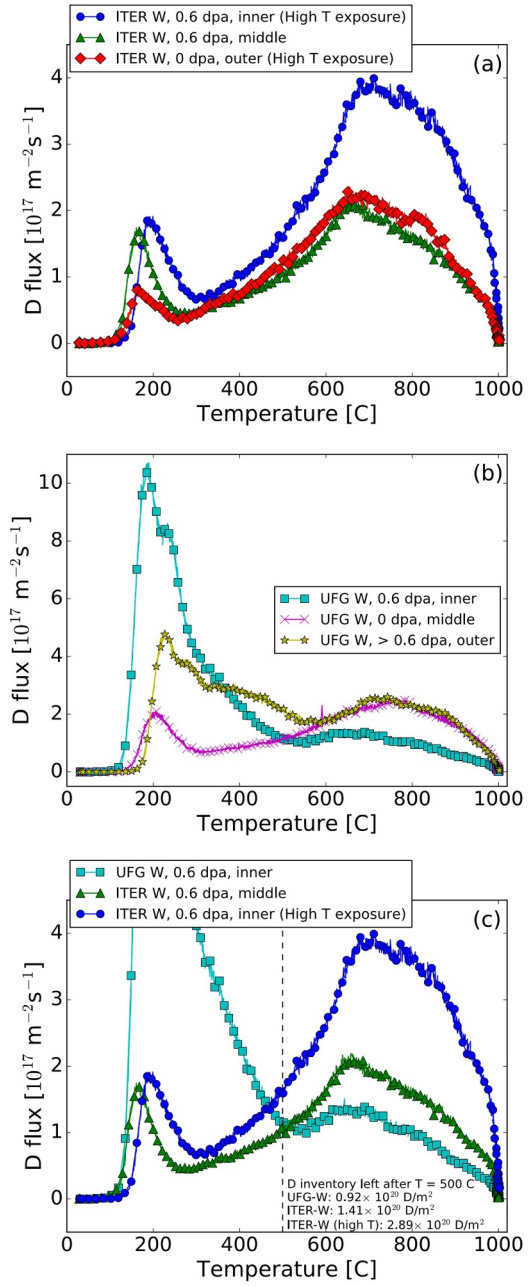

Fig. 6. Thermally desorbed D fluxes for the ITER grade W samples (a), the UFG W samples (b), and a comparison of samples with similar temperature histories and/or damage (c). UFG W samples tend to release most of their trapped D at lower temperatures; whereas, most of the ITER grade W inventory is released at temperature above 500 °C. (For clarity, the TDS data for the UFG W 0.06 dpa sample is not shown, since it was measured with the electron multiplier off.).

profiles of D, it does not provide a measurement of the types of defects where the D atoms are trapped. As a result, we rely on TDS to provide more insight into the binding energies of D to traps in our ion damaged specimens.

The TDS spectra depicted in Fig. 6 show the D release from the sample as the temperature increases. During the heating process, D is liberated from traps and diffuses to the surface. It then recombines with H or another D and desorbs as a molecule where it is finally detected by our mass spectrometer. It is common practice to simulate desorption spectra using a 1-D diffusional model [2,30]. By fitting the intensities and positions of the desorption peaks, it is possible to calculate the corresponding trap energies and concentrations. However, applying such a model in this case is challenging for several reasons. Unlike in a steady state linear plasma device, the exposure conditions in the DIII-D divertor are much more complex, with rapid variations in temperature and ion flux in each shot. In addition, the exact nature of potential D trapping sites within the UFG W has yet to be rigorously determined using microscopy. Given these limitations, we will instead qualitatively describe the D release data and defer detailed modeling of these results until a future study.

Fig. 6a shows the desorption spectra of the ITER grade W samples. In all cases, two distinct desorption peaks appear at approximately 190 °C and 700 °C. This result is consistent with previously published W retention studies where samples are about 200 °C during plasma exposure [4,26]. The intensity of the release peak at 190 °C is significantly higher for the two specimens pre-damaged to 0.6 dpa. This trend is inconclusive for the 700 °C desorption peak, where the desorbed D flux is increased for only one the 0.6 dpa samples in comparison with the undamaged case. This difference likely can be ascribed to the different temperature histories for these samples. In addition to simple trapping at defects produced by ion damage, it is also plausible that some of the D precipitates in molecular form within gas-filled bubbles or blisters that form due to plasma exposure. Precipitation of molecular D_2 is thermodynamically favorable in materials such as W where the dissolution of D within the lattice is highly endothermic [29], and such structures have been observed to form in ITER-grade W [18].

In Fig. 6b, we show TDS spectra for the UFG W specimens. These spectra are characterized by desorption peaks at 200 °C and 650–750 °C, at temperatures that are similar to the ITER grade W samples. Additional release peaks for the damaged UFG specimens appear at 250 °C, along with the tail end another broad peak around 300–350 °C. This suggests that displacement damage in UFG W may create traps that more weakly bind D than in ITER grade W. From the TDS data in Figs. 6a-b, ion-damaged ITER grade W exhibits elevated D release at both of the main desorption temperatures of 200 °C and 850 °C, whereas pre-damaging the UFG W enhances desorption only at lower temperatures. The best source of comparison are the samples with the closest temperature histories and damage levels. Fig. 6c illustrates the TDS spectra of the ITER grade and UFG W specimens ion damaged to 0.6 dpa (corresponding to the bold-face entries in Table 1.) For comparison, we also show the other ITER grade W sample damaged to 0.6 dpa to highlight the effect of higher temperature exposure. In Fig. 6c, we also indicate the amount of D remaining in each specimen after baking to 500 °C by integrating the TDS spectra up to this point. After the 500 °C point in the thermal desorption is reached, the ITER grade specimens have 1.5–3 times more remaining trapped D than the UFG W sample. Although the ion-damaged UFG W retains much more D initially, most of this is released below 500 °C.

One other aspect of D retention in the UFG W that must also be addressed is the effect of the TiO_2 dispersoids. Because Ti is well-known to form a hydride phase under appropriate conditions, concern about elevated retention in the dispersoids themselves is reasonable. Prior work by Caskey [31] indicates that TiO_2, on the other hand, does not have a high affinity for hydrogen. We do not know, however, what effect the 12 MeV Si ion damage has on the dispersoids themselves. It was not possible to index the dispersoids during EBSD analysis, and XRD did not reveal conclusive evidence of their crystal structure [18], indicating that these particles may be nearly amorphous in structure. Oxide-matrix interfaces have been shown to affect damage accumulation behavior during ion irradiation. This could bias D trapping to these interfaces over grain boundaries.

We summarize our data in Table 1 to emphasize the main retention results. The sample name, location, dpa and total retention (from TDS data) are shown. In addition, we include two results that illustrate the main differences we find in UFG W. We first calculate the percentage of D trapped within the 3 μm depth limit of the NRA analysis. This is accomplished by taking the ratio of the integrated NRA retention profile and the total retention measured from TDS. (Note that this assumes that

all D within the sample is released during thermal desorption up to 1000 °C.) Based on this analysis, we note that 0.6 dpa UFG W retains 86–100% of its trapped D within this 3 μm depth, compared with 39–61% for the 0.6 dpa ITER-grade specimens. This suggests that UFG W has a much higher trap (lattice defect) density, which may serve to limit diffusion/trapping at greater depths. As was done for Fig. 6c, we also calculate the amount of D remaining in each specimen after annealing to 500 °C, now for all specimens. The undamaged UFG W retains slightly more D than ITER grade W after baking up to 500 °C. However, UFG W pre-damaged to 0.6 dpa releases a larger fraction (50–77%) of its trapped D inventory by heating to this temperature. This suggests that in a practical magnetic confinement device, low-temperature heating could be used as an avenue to limit tritium inventory in damaged UFG W.

4. Summary

In this work, we have studied D retention in ITER grade and UFG tungsten with varying levels of 12 MeV Si ion damage following exposure to divertor plasma in DIII-D. Undamaged specimens were included in our test matrix for reference, and damage levels up to 0.6 dpa were considered. All samples were exposed to ten similar L-mode discharges using the DiMES platform, followed by quantification of retained D using NRA and TDS. We find that for similar levels of ion damage, UFG W consistently retains more D than ITER grade W. However, the complete picture is more nuanced, as illustrated by our TDS characterization. For both microstructures, the D release rate reaches maxima at 200 °C and 750 °C. However, pre-damaging the samples affects each material differently. In UFG W, the 200 °C peak is strongly enhanced, while the high temperature (750 °C) peak is only modestly affected. The reverse appears to be true of the ITER grade specimens. An analysis of NRA and TDS data indicates the UFG W pre-damaged to 0.6 dpa retains 86–100% of its trapped D within the first 3 μm of the surface, compared 39–61% for the 0.6 dpa ITER-grade specimens.

Optimizing a material to enhance specific properties can result in compromises in other aspects of its desired performance, and ultimately we must determine whether elevated tritium retention is an acceptable trade-off if other benefits are realized. While the answer to this question depends on many factors, based on the results of this study we note that the penalty of increased D retention in the UFG W is still within the spread of values available in the literature for ITER-grade, recrystallized, and single crystal tungsten microstructures [32,33]. Furthermore, our results suggest that much of the trapped inventory can be recovered with low temperature baking, an option that could plausibly be implemented in a practical reactor design. Taking these factors into account, UFG tungsten materials are certainly worthy of continued study to more completely evaluate their strengths and weaknesses. One issue that must be considered is how small changes in exposure temperature and dpa level can significantly affect diffusion and trapping. Further work using better controlled laboratory plasma discharges presents an avenue to deciphering the differences in retention we observed. In addition, detailed microscopy studies are suggested to provide insight into the defects responsible for hydrogen isotope retention. Such work will also help simplify modeling of the TDS and NRA results to quantify trapping energies and better understand hydrogenic diffusion in ITER grade W, as has been done in other prior work [2,4,30].

Declaration of interests

The authors declare that they have no known competing financial interests or personal relationships that could have appeared to influence the work reported in this paper.

Acknowledgments

Sandia is a multi-program laboratory managed and operated by Sandia Corporation, a wholly-owned subsidiary of the Honeywell Corporation, for the United States Department of Energy's National Nuclear Security Administration under contract DE-NA0003525. This work was also supported by our coauthors under Department of Energy contracts DE-FG02-07ER54917, DE-AC52-07NA27344, DE-AC05-000R22725, and DE-FC02-04ER54698.

Supplementary materials

Supplementary material associated with this article can be found, in the online version, at doi:10.1016/j.nme.2019.100689.

References

[1] R.A. Causey, Hydrogen isotope retention and recycling in fusion reactor plasma-facing components, J. Nucl. Mater. 300 (2–3) (2002) 91–117.
[2] M. Shimada, G. Cao, Y. Hatano, T. Oda, Y. Oya, M. Hara, P. Calderoni, The deuterium depth profile in neutron-irradiated tungsten exposed to plasma, Phys. Scr. T145 (2011) 014051.
[3] V. Philipps, Tungsten as material for plasma-facing components in fusion devices, J. Nucl. Mater. 415 (1) (2011) S2–S9.
[4] J.L. Barton, Y.Q. Wang, R.P. Doerner, G.R. Tynan, Model development of plasma implanted hydrogenic diffusion and trapping in ion beam damaged tungsten, Nucl. Fusion 56 (106030) (2016) 17pp.
[5] M. Shimada, G. Cao, T. Otsuka, M. Hara, M. Kobayashi, Y. Oya, Y. Hatano, Irradiation effect on deuterium behaviour in low-dose HFIR neutron-irradiated tungsten, Nucl. Fusion 55 (2015) 0130089pp.
[6] M. Shimada, Y. Hatano, P. Calderoni, T. Oda, Y. Oya, M. Sokolov, K. Zhang, G. Cao, R. Kolasinski, J. Sharpe, First result of deuterium retention in neutron-irradiated tungsten exposed to high flux plasma in TPE, J. Nucl. Mater. 415 (1, Supplement) (2011) S667–S671.
[7] Y. Hatano, M. Shimada, T. Otsuka, Y. Oya, V. Kh. Alimov, M. Hara, J. Shi, M. Kobayashi, T. Oda, G. Cao, K. Okuno, T. Tanaka, K. Sugiyama, J. Roth, B. Tyburska-Püschel, J. Dorner, N. Yoshida, N. Futagami, H. Watanabe, M. Hatakeyama, H. Kurishita, M. Sokolov, Y. Katoh, Nucl. Fusion 53 (2013) 073006.
[8] J. Riesch, T. Höschen, Ch. Linsmeier, S. Wurster, J-H You, Enhanced toughness and stable crack propagation in novel tungsten fibre-reinforced tungsten composites produced by chemical vapour infiltration, Phys. Scr. T159 (2014) 14031.
[9] A. Autissier, M. Richou, L. Minier, F. Naimi, G. Pintsuk, F. Bernard, Spark plasma sintering of pure and doped tungsten plasma facing material, Phys. Scr. T159 (2014) 014034.
[10] N. Lemahieu, J. Linke, G. Pintsuk, G. Van Oost, M. Wirtz, Z. Zhou, Performance of yttrium doped tungsten under 'edge localized mode' -like loading conditions, Phys. Scr. T159 (2014) 014035.
[11] H. Kurishita, S. Matsuo, H. Arakawa, T. Sakamoto, S. Kobayashi, K. Nakai, H. Okano, H. Watanabe, N. Yoshida, Y. Torikai, Y. Hatano, T. Takida, M. Kato, A. Ikegaya, Y. Ueda, M. Hatakeyama, T. Shikama, Current status of nanostructured tungsten-based materials development, Phys. Scr. T159 (2014) 014032.
[12] C. Ren, M. Koopman, Z.Z. Fang, H. Zhang, B. van Devener, A study on the sintering of ultrafine grained tungsten with Ti-based additives, Int. J. Refract. Metals Hard Mater. 65 (2017) 2–8.
[13] M. Zibrov, M. Mayer, E. Markina, K. Sugiyama, M. Betzenbichler, H. Kurishita, Yu. Gasparyan, O.V. Orgorodnikova, A. Manhard, A. Pisarev, Deuterium retention in TiC and TaC doped tungsten under low-energy ion irradiation, Phys. Scr. T159 (2014) 014050.
[14] O. El-Atwani, S. Gonderman, M. Efe, G. De Temmerman, T. Morgan, K. Bystrov, D. Klenosky, T. Qiu, J.P. Allain, Ultrafine tungsten as a plasma-facing component in fusion devices: effect of high flux, high fluence low energy helium irradiation, Nucl. Fusion 54 (8) (2014) 083013.
[15] G. Pintsuk, H. Kurishita, J. Linke, H. Arakawa, S. Matsuo, T. Sakamoto, S. Kobayashi, K. Nakai, Thermal shock response of fine- and ultra-fine-grained tungsten-based materials, Phys. Scr. T145 (2011) 0140605pp.
[16] K. Tokunaga, H. Kurishita, H. Arakawa, S. Matsuo, T. Hotta, K. Araki, Y. Miyamoto, T. Fujiwara, K. Nakamura, T. Takida, M. Kato, A. Ikegaya, High heat load properties of nanostructured, recrystallized W–1.1TiC, J. Nucl. Mater. 442 (1–3) (2013) S297–S301.
[17] A. Suslova, O. El-Atwani, D. Sagapuram, S.S. Harilal, A. Hassanein, Recrystallization and grain growth induced by ELMs-like transient heat loads in deformed tungsten samples, Sci. Rep. 4 (1) (2014) 6845.
[18] R.D. Kolasinski, D.A. Buchenauer, R.P. Doerner, Z.Z. Fang, C. Ren, Y. Oya, K. Michibayashi, R.W. Friddle, B.E. Mills, High-flux plasma exposure of ultra-fine grain tungsten, Int. J. Refract. Metals Hard Mater. 60 (2016) 28–36.
[19] D.A. Buchenauer, R.A. Karnesky, Z.Z. Fang, C. Ren, Y. Oya, T. Otsukad, Y. Yamauchie, J.A. Whaley, Gas-driven permeation of deuterium through tungsten and tungsten alloys, Fusion Eng. Des. 111 (2016) 104–108.
[20] ITER Materials Assessment Report, ITER Doc. G74 MA 10 01-07-11 W 0.2, 2001.

[21] K.P. Mingard, B. Roebuck, E.G. Bennett, M.G. Gee, H. Nordenstrom, G. Sweetman, P. Chan, Comparison of EBSD and conventional methods of grain size measurement of hard metals, Int. J. Refract. Met. Hard Mater 27 (2) (2009) 213–223.
[22] W.R. Wampler, D.L. Rudakov, J.G. Watkins, C.J. Lasnier, The influence of displacement damage on deuterium retention in tungsten exposed to divertor plasma in DIII-D, J. Nucl. Mater. 415 (1) (2011) S653–S656.
[23] J.F. Ziegler, SRIM, http://www.srim.org (2013).
[24] P.C. Stangeby, The Plasma Boundary of Magnetic Fusion Devices, IOP publishing, 2000.
[25] M. Mayer, SIMNRA User's Guide, Max-Planck-Institut für Plasmaphysik, Garching, Germany, 1997 Report IPP 9/113.
[26] M.J. Simmonds, Y.Q. Wang, J.L. Barton, M.J. Baldwin, J.H. Yu, R.P. Doerner, G.R. Tynan, Reduced deuterium retention in simultaneously damaged and annealed tungsten, J. Nucl. Mater. 494 (2017) 67–71.
[27] H. Eleveld, A. van Veen, Deuterium interaction with impurities in tungsten studied with tds, J. Nucl. Mater. 191-194 (1992) 433–438.
[28] Y. Liu, Y. Zhang, H. Zhou, G. Lu, F. Liu, G. Luo, Vacancy trapping mechanism for hydrogen bubble formation in metal, Phys. Rev. B 79 (17) (2009) 172103.
[29] W. Wampler, R. Doerner, The influence of displacement damage on deuterium retention in tungsten exposed to plasma, Nuclear Fusion 49 (11) (2009) 115023.
[30] J.H. Yu, M. Simmonds, M.J. Baldwin, R.P. Doerner, Deuterium desorption from tungsten using laser heating, Nuclear Mater. Energy 12 (2017) 749–754.
[31] G.R. Caskey, Diffusion of tritium in rutile (TiO_2), Mater. Sci. Eng. 14 (1974) 109.
[32] A. Manhard, K. Schmid, M. Balden, W. Jacob, Influence of the microstructure on the deuterium retention in tungsten, J. Nucl. Mater. 415 (1) (2011) S632–S635.
[33] M. Balden, A. Manhard, S. Elgeti, Deuterium retention and morphological modifications of the surface in five grades of tungsten after deuterium plasma exposure, J. Nucl. Mater. 452 (1–3) (2014) 248–256.